Original Article

IJCIH
Converging Healthcare & Technology

INTERNATIONAL JOURNAL OF CONVERGENCE IN HEALTHCARE

Published by
IJCIH & Pratyaksh Medicare LLP

www.ijcih.com

Study of Structural Modification in $YBa_2Cu_3O_{7-y}$ + x Sb_2O_3 Superconductor Composite

M. Sahoo[1], D. Behera[2]

[1]Teaching Resource Person, Department of Physics, Gurugram University, Gurugram-122003, [2]Professor, Department of Physics and Astronomy, National institute of Technology, Rourkela-769008

Abstract

A series of $YBa_2Cu_3O_{7-y}$ + x Sb_2O_3 (x = 0.0, 0.01, 0.03, 0.05, 0.08, 0.2 wt. %) samples were prepared using the solid state reaction method. The structural disorder has been studied using XRD and Raman techniques. XRD graphs show the unchanged orthorhombic structure. The increase in peak width of the XRD pattern in the composites signifies the decrease in crystallite size with Sb_2O_3 addition. Raman analysis confirms all the vibration modes in pure YBCO along with some peaks of antimony. The structural changes are marked by peak sifting in the XRD pattern and the softening in the Raman modes. Linear relation is portrayed between oxygen content and the c axis lattice parameter. The c axis tends to increase with the decrease in oxygen content as calculated from XRD and Raman data. EDX analysis shows the incorporation of Sb_2O_3 to grain boundary region along with the presence of all the compositional elements. Microstructure analysis has been studied through SEM. SEM graphs shows that pristine YBCO exhibits large and elongated grains randomly oriented in all directions. The grain size decrease in low wt. % addition of Sb_2O_3 and increase in higher wt. % addition.

Keywords: *HTSC, RAMAN, Electrical conductivity, Grain boundary, Microstructure.*

Introduction

Even after several decades of research on high T_c superconductors (HTSC), these materials are still interesting for many researchers. In recent years there have been intense theoretical and experimental activities in the investigation of the copper oxide based high T_c superconductors[1-3]. Bulk HTSC samples are granular in nature, characterized by the presence of grains and twin boundaries, secondary phases and other less important defects. Thus, granular superconductors can be considered as disordered systems formed by anisotropic grains weakly coupled and randomly distributed, where we can distinguish two main contributions to their properties. The first one, called intra-grain contribution, is associated with high critical current density values and grains completely shielded at sufficiently low magnetic fields. The second one, called inter-grain contribution, is characterized by lower critical current density values associated to Josephson couplings. Thus, the granularity arising from this structure, is responsible for the typical low J_c values of HTSC and for their strong dependence with temperature and applied magnetic field. Therefore, the inter-grain material has an important role in the technological applications of HTSC, in particular in the presence of

Corresponding Author:
M. Sahoo
Teaching Resource Person, Department of Physics,
Gurugram University, Gurugram-122003
e-mail: sahoomousumi0@gmail.com

magnetic fields [4-6]. The planes containing copper and oxygen atoms that are chemically bonded to each other have a crucial importance in YBCO. The special nature of the copper-oxygen chemical bond contributes to an effective electrical conductivity in certain directions. The existence of the Cu-O chains and the CuO_2 planes in cuprate superconductors indicates the important role of Cu atoms. Thus, the ionic radius as well as the valence number of the dopant element has a crucial role in determining the characteristics of new superconductors. Doping of YBCO with various elements is conducted for two basic purposes. The first one is the modification of the microstructure in order to obtain fundamental information related to the possible mechanisms, and the second one is to improve its physical characteristics. It has been seen that substitutions at the Y and Ba sites does not generate any discernible effect, while substitution at the Cu and O sites has significant effects on the superconducting properties of cuprates[7]. Due to the low melting point and the possible surfactant action of semi-metallic Sb_2O_3 doping, it is expected that doping with Sb could improve the grain boundary characteristics and enhance the inter-granular coupling in Y123. Paulose et al.[8] reported that Sb_2O_3 doping significantly increases the rate of oxygen absorption in the Y123 system. Jin et al.[9] determined that Sb_2O_3 doping of Y123 improves the value of the critical current density, J_c, along with a decrease in T_c and a reduction in grain size with increasing porosity. Also Vlakhov [10] reported that even small doping levels of Sb shift the step of J_c (B) dependence to higher magnetic fields but cannot improve the weak link behaviour.

Experimental Procedure: YBCO powder is prepared by the solid state reaction route by mixing stoichiometry amount of Y_2O_3, $BaCO_3$, CuO followed by grinding, calcination at 900^0 C, sintering at 920^0C and annealing at 500^0C for 8 hrs for oxygen uptake respectively. A series of polycrystalline composite samples of (1-x) YBCO + x Sb_2O_3 (x = 0.0, 0.01, 0.03, 0.05, 0.08, 0.2 wt. %) were ground and pressed into pellets. The composite pellets were sintered at 920^0 C for 12 hours and then cooled to 500^0 C where they were kept for 5 hours in an oxygen atmosphere for oxygen intake. Phase confirmation and structural analysis were done by X-ray powder diffraction technique (Rigaku Ultima IV set-up). Raman study was done to confirm the vibrational modes (Renisaw invia, Laser (514nm & 785nm) with Leica microscopy DM-2500M). The grain morphology of the samples was analyzed by scanning electron microscope (Model No. JSM-6480 LV, Make JEOL) and the compositional analysis was determined by energy dispersive X-ray analysis (EDX) using an INCA Oxford Analyzer attached to a scanning electron microscope.

Results and Discussion

XRD Analysis: Figure 1 shows the X-ray diffraction patterns of the $YBa_2Cu_3O_{7-y}/xSb_2O_3$ composite samples. The diffraction pattern of all the samples is indexed using ChekCell software and the results are found to be in orthorhombic phase with a space group P_{mmm}, with some Sb_2O_3 peaks. The lattice parameters and unit cell volumes of these samples are presented in Table1.

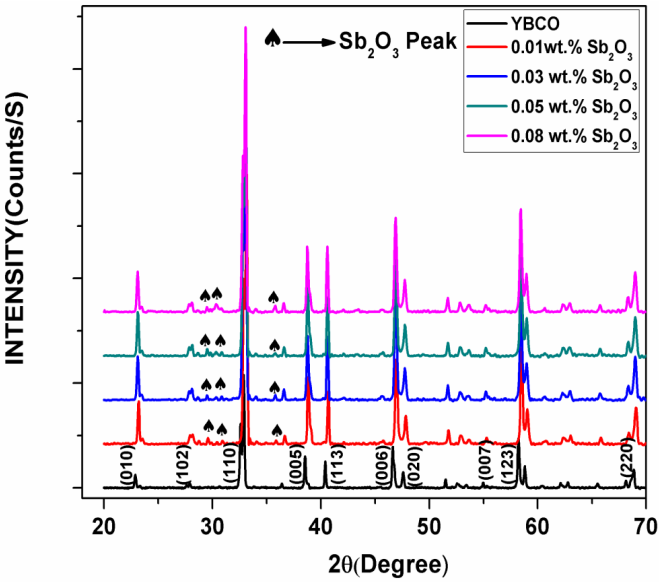

Figure 1. XRD Patterns of YBCO+ x Sb_2O_3 Samples (x = 0.0, 0.01, 0.03, 0.05, 0.08 wt. %).

Figure 2 shows magnified (005) and (006) planes. The peak intensity increases monotonically for Sb_2O_3 added samples. The clear sifting of the peak position to the higher angle side is visible in all the composite samples. Basically the crystallite size is reflected in the broadening of a particular peak in a diffraction pattern associated with a particular planar reflection from within the crystal unit cell. It is inversely related to the FWHM of an individual peak. The narrower the peak, the larger the crystallite size. The FWHM value is smaller in the pristine sample as compared to the composite samples. The peak width little bit increases in the composites which signifies the decrease in crystallite size with Sb_2O_3 addition.

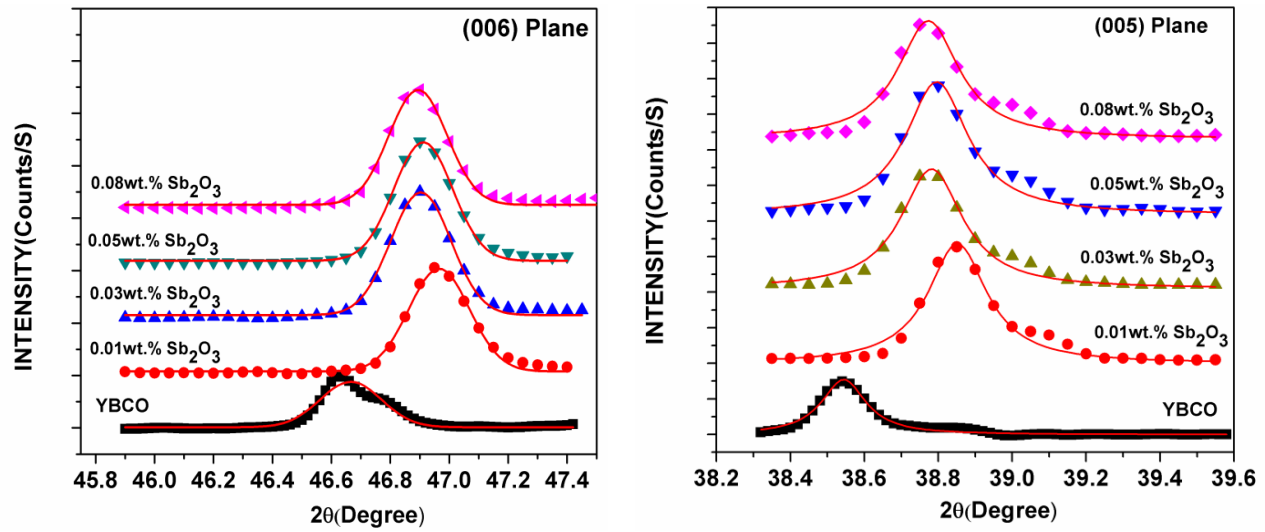

Figure 2. Lorentzian fitting of (005) and (006) plane plotted by varying Sb_2O_3 wt.%.

Table 1. Parameters calculated from XRD graphs

Sb_2O_3(wt.%)	a (A^0)	b (A^0)	c (A^0)	V(A^{03})	Anisotropy
YBCO	3.818(1)	3.884(1)	11.681(2)	173.218	1.7
0.01	3.824(3)	3.885(2)	11.703(5)	173.862	1.5
0.03	3.818(2)	3.874(1)	11.728(7)	173.468	1.4
0.05	3.804(2)	3.884(1)	11.686(6)	172.657	2.0
0.08	3.813(1)	3.871(1)	11.658(4)	172.073	1.5

The length of 'b' parameter remains almost same in the composite samples except the 0.03 and 0.05 wt.% Sb_2O_3 added sample, where the length decreases slightly. The length of 'c' parameter is higher in the composite samples as compared to the pristine sample except the highest wt.% added sample where the length decreases slightly. For low oxygen content sample, the c-axis length is high. The oxygen stoichiometry value is calculated from the relation 7-y = 75.250-5.856c (presented in Table 2) where c is the c-axis lattice parameter [11]. The anisotropy, Anis =100 (b-a)/0.5 (b+a) which is the percentage deviation from tetragonal structure is calculated and listed in Table 1. The anisotropy is 1.7 for pristine and highest for 0.05 % Sb_2O_3 added sample.

RAMAN analysis: Raman spectroscopy is a characterization method that measures the frequencies of the long-wavelength lattice vibrations (phonons). Figure 3 shows the Raman spectrum of YBCO + x Sb_2O_3 (x = 0.0, 0.01, 0.03, 0.05, 0.08 wt. %) composite samples. A perovskite YBCO unit cell has five different oxygen sites which get activated under the influence of photons: O (1) in CuO chains, O(2,3) in CuO_2 planes, O(4) in the apical chains and O(5) lies in between the oxygen chains which is empty in orthorhombic structure. The active vibration along the c axis are shown at peak position 500 cm^{-1}, 432 cm^{-1}, 339 cm^{-1}. 500 cm^{-1} represents the stretching of apical oxygen or the bridging oxygen O(4) denoted as $O(4)A_g$. 432 cm^{-1} represents in phase vibration of O (2)– O(3) oxygen atom in CuO_2 plane marked as $O(2,3)A_g$ and 339 cm^{-1} represents out-of-phase c axis vibration of O(2)-O(3) oxygen atom in CuO_2 plane labeled as O(2,3) B_{1g} [12-15]. The other two Raman active modes are vertical along the c axis given by Cu (2) atoms (151 cm^{-1}) denoted as Cu (2) A_g i.e plane Cu in phase and Ba atoms (115 cm^{-1}) marked BaA_g i.e Ba vibration. The strong peak of 500 cm^{-1} at y=0 shifts to the lower frequency side as the oxygen content decreases. In addition, the 115 cm^{-1} peak of the y = 0 sample disappears at 7-y = 6.2[16].

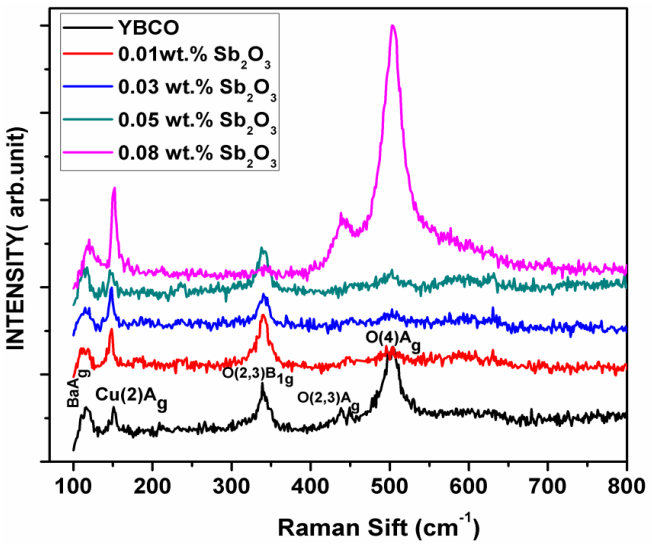

Figure 3. Micro-Raman spectra of YBCO + x Sb_2O_3 Samples (x = 0.0, 0.01, 0.03, 0.05, 0.08 wt.%) samples.

From the Raman graphs (fig3) it is clear that all the vibrational modes are present in the pristine YBCO as well as in the composite samples. The 500 cm^{-1} peak softens in 0.01, 0.03, 0.05 wt.% added samples and hardens for the highest Sb_2O_3 %. Also the 115 cm^{-1} and 151 cm^{-1} peaks hardens in the highest wt.% composite sample. There are some extra modes detected in the doped samples. These are at 188cm^{-1}, 595cm^{-1}, 243cm^{-1} for 0.01 %, 596 cm^{-1} for 0.03 %, 241 cm^{-1}, 595cm^{-1} for 0.05 % and at 213 cm^{-1} for 0.08 % Sb_2O_3 added samples. These modes are found to be of Sb_2O_3. Generally, the two common forms of Sb_2O_3 are the cubic phase senarmontite and the orthorhombic phase valentinite. It has signals at 82, 118, 141, 189, 219, 254, 295, 355, 373, 450, 500, 596, 684, 712, and 904 cm^{-1}. All signals below 400 cm^{-1} belong to the external lattice mode regime, while those above 400 cm^{-1}' belong to the internal vibrations [17,18]. Generally, the O4 phonon mode, is associated with the oxygen content y. Huong et al. proposed the following relationship between the oxygen content and the peak frequency of the O4 mode as,[19]

$$y = 13.58 - 0.027\nu$$

where ν is the peak frequency of the O4 mode.

Table 2: Different parameters calculated using XRD and Raman spectra. 'c' is lattice parameter along Z direction, y is oxygen loss, ν is frequency of apical oxygen.

Sb_2O_3 (wt.%)	c (A^0)	O_{7-y} (from XRD)	ν(cm^{-1})	O_{7-y} (from Raman)
0.00	11.681(2)	6.85	504	7.02
0.01	11.703(5)	6.71	498	6.86
0.03	11.728(7)	6.57	502	6.97
0.05	11.686(6)	6.82	502	6.97
0.08	11.658(4)	6.98	504	7.02

Linear relation is portrayed between oxygen content and the c axis lattice parameter. The c axis tends to increase with the decrease in oxygen content. Table 2 shows the oxygen content (y) evaluated using frequency of Raman mode and the c axis of XRD. It gives an insight of oxygen suppression occurring on the apical site and lengthening of the c axis due to Sb_2O_3 addition. Another thing was noticed here is that, even if the oxygen value remains high in all the pure as well as composite samples, the T_c value reduces to a large extent in the Sb_2O_3 added samples. This signifies that the oxygen concentration is not the predominant factor for high T_c superconductivity in YBCO system. Its role is to adjust the coupling strength between positive and negative ions.

Microstructural analysis: The grain size distribution of the pristine and doped samples are shown in figure 4. It shows that pristine YBCO exhibits large and elongated grains randomly oriented in all directions. For 0.01 and 0.03 wt.% addition of Sb_2O_3 the grain size decreases to a greater extent. But further increase of Sb_2O_3 addition, the grain size increases and also the porosity increases.

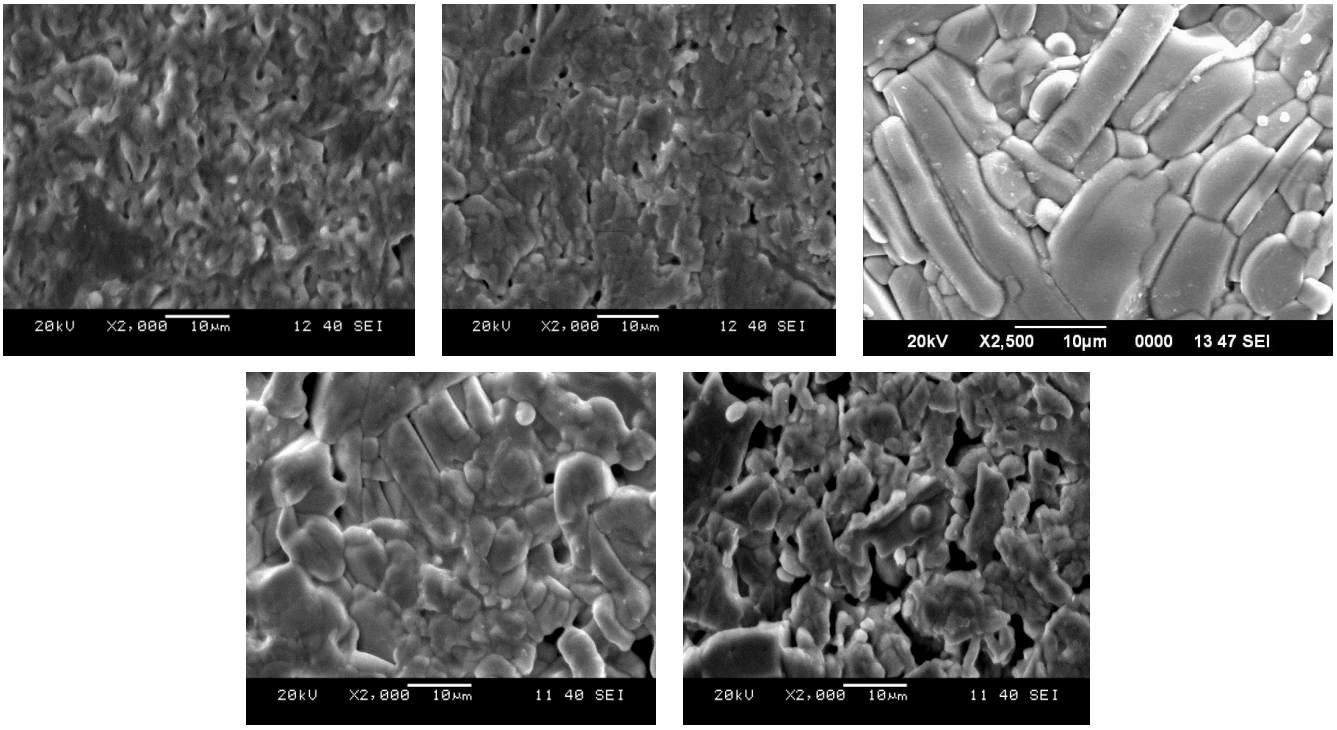

Figure. 4 SEM micrographs of YBCO + x Sb_2O_3 (x = 0.0, 0.01,0.03,0.05,0.08 wt.%) marked as a, b, c, d, e respectively.

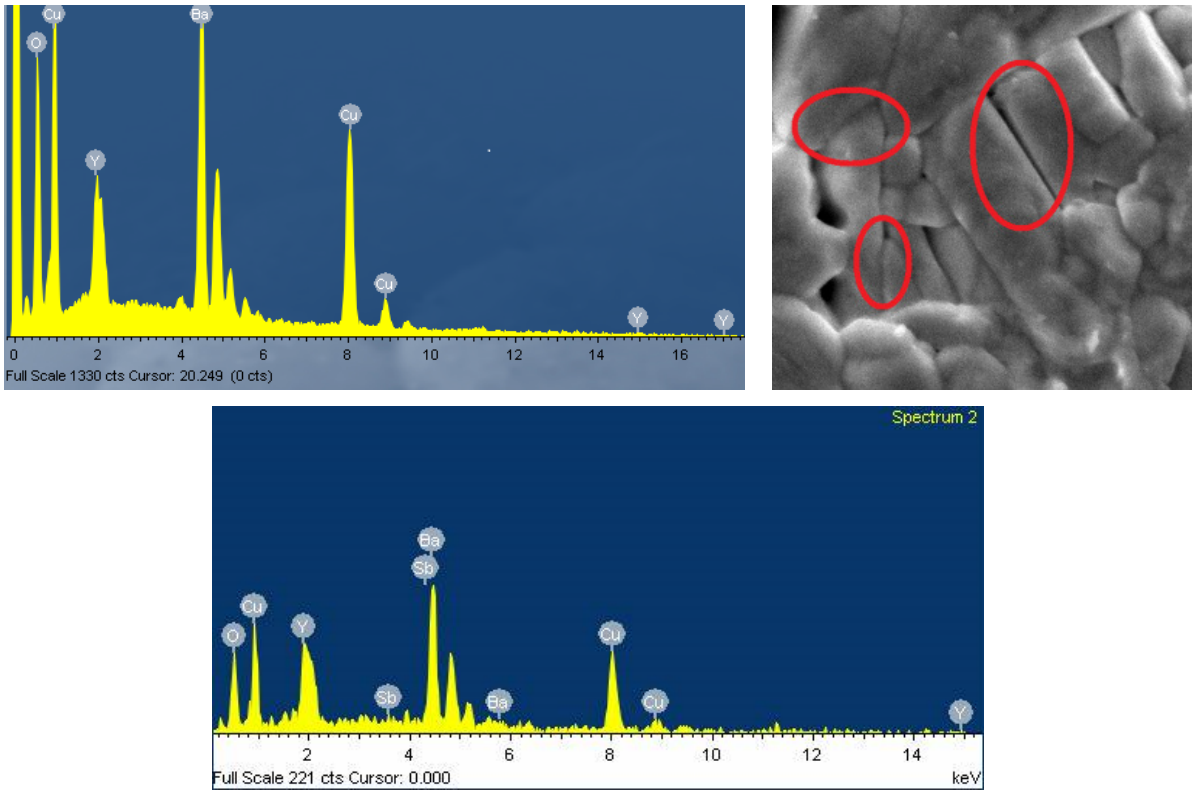

Figure 5. EDX graphs of YBCO and 0.05 % Sb_2O_3 added sample (taken at the grain boundary region) marked as a and b respectively.

The presence of all the compositional elements in the pristine as well as in doped samples is confirmed from the EDX graphs. The EDX taken at the grain boundaries clearly shows the presence of Sb at the boundaries (shown by red circles in the inset SEM fig. 5b). It indicates that some amount of the added antimony goes to the grain boundary region in addition of its incorporation to inside grains, which enhances the inter-grain coupling which is also observed in the R-T plots.

Conclusion

The effect of semiconductor Sb_2O_3 on the structural property is studied. XRD graphs show the unchanged orthorhombic structure in the composite samples. Raman studies show all the vibrational modes in the pristine as well as composite samples in addition to presence of Sb_2O_3 modes. The structural changes are marked by peak sifting in the XRD pattern and the softening in the Raman modes. SEM micrographs show reduced grain size in low % addition of Sb_2O_3 and grain size increases for the high % addition of Sb_2O_3. EDX analysis shows the incorporation of Sb_2O_3 to grain boundary region along with the presence of all the compositional elements.

Conflict of interest: There is no conflict of interest.

Source of Funding: This work is self-funded.

Ethical Clearance: NA

References

1. Dagotto E, Correlated electrons in high-temperature superconductors, Rev. Mod. Phys. 1994; 66: 763-840.
2. Kampf A P, Magnetic correlations in high temperature superconductivity, Phys. Rep.1994; 249: 219-351.
3. Scalapino D J, The case for d $_{x2-y2}$ pairing in the cuprate superconductors, Phys. Rep.1995; 250: 329-365.
4. Araujo-Moreira F M, Ortiz W A, De Lima O F, Multilevel granular structure and its coupling distribution in melt-textured $YBa_2Cu_3O_{7-x}$, Physica C 1999; 311: 98-106.
5. Araujo-Moreira F M, Ortiz W A, De Lima O F, Study of the intergranular and intra-granular characteristics in a melt-textured-growth sample of $YBa_2Cu_3O_{7-x}$, Physica C 1994; 3205: 235-240.
6. Araujo-Moreira F M, Ortiz W A, De Lima O F, Exponential critical state model applied to ac susceptibility data for the superconductor $YBa_2Cu_3O_{7-\delta}$, J. Appl. Phys. 1996; 80: 3390.
7. Skakle J M S, Crystal chemistry substitutions and doping of $YBa_2Cu_3O_x$ and related superconductors, Mater. Sci. Eng. R 1998; 23: 1-40.
8. Paulose K V, Koshy J, Uma Devi P, Damodaran A D, High temperature superconductivity in air quenched $YBa_2Cu_3O_{7-\delta}$ doped with Sb_2O_3, Appl.Phys. Lett. 1991; 59: 1251–1253.
9. Jin S, Tiefel T H, Fastnacht R A, Kammlott G W, Critical current behaviour in the Sb_2O_3-doped $YBa_2Cu_3O_{7-\delta}$ superconductor, Appl. Phys. Lett. 1992; 60: 3307-3309.
10. Vlakhov E, Gattef E, Dimitriev Y, Staneva A, Synthesis and superconductivity of $YBa_2Cu_3O_y$ ceramics doped with Sb, Ag and Te, J. Mater. Sci. Lett. 1994; 13:1654-1656.
11. Benzi P, Bottizzo E, Rizzi N, Oxygen determination from cell dimensions in YBCO superconductors, J. Crystal Growth 2004; 269: 625-629.
12. Liu R, Thomsen C, Kress W, et al, Frequencies, eigenvectors, and single-crystal selection rules of k=0 phonons in $YBa_2Cu_3O_{7-\delta}$: Theory and experiment, Phys. Rev. B 1988; 37: 7971-7974.
13. Cohen R E, Pickett W E, Krakauer H, Theoretical determination of strong electron-phonon coupling in $YBa_2Cu_3O_7$, Phys. Rev. Lett.1990;64: 2575-2578.
14. Rodriguez C O, Lichtenstein A I, Mazin I I et al, Phys. Rev. B 1990; 42: 2692.
15. Prade J, Kulkarni A D, de Wette F W et al, Phys. Rev. B1990; 39: 2771.
16. Yamanaka A, Minami F, Watanabe K et al, Jpn. J. Appl. Phys. 1987; 26: L1404.
17. Cody C A, Dicarlo L, Darlington R K, Vibrational and thermal study of antimony oxides, Inorg. Chem.1979; 18:1572-1576.
18. Mestl G, Ruiz P, Delmon B, Knozinger H, Sb_2O_3/ Sb_2O_4 in Reducing/Oxidizing Environments: An in Situ Raman Spectroscopy Study, J. Phys. Chem.1994; 98: 11276-11282.
19. Huong P V, Bruyere J C, Bustarret E, Granchampb P, Solid State Commun. 1989;72: 191.